WIND TUNNEL TESTS OF AN ULTRALIGHT SAILPLANE WING SECTION

by D.J. Marsden

University of Alberta, Canada

Presented at the XXI OSTIV Congress, Wiener-Neustadt, Austria (1989)

Summary

The UAG 88-143/20 wing section was designed for use on an ultralight sailplane wing that would require good performance at low Reynolds number. A model was tested in the University of Alberta low turbulence wind tunnel at Reynolds numbers of 0.5×10^6, 1.0×10^6 and 2.1×10^6 with camber flap at 0°, +10°, and −10°. Tests were repeated with simulated insect roughness to check on sensitivity to roughness.

The measured results were interpolated to present drag polars for flight Reynolds number which would occur for any given sailplane geometry. Curves were drawn to represent wing tip, wing root and mean chord Reynolds number with and without water ballast.

The new wing section has excellent lift-drag characteristics, particularly at lift coefficients in the range from 0.5 to 1.5, and at low Reynolds number. It displays very docile stall characteristics that will enhance flight safety. Sensitivity to roughness was low, particularly at the lower Reynolds numbers.

The new section should be suitable for the proposed ultralight sailplane.

Introduction

The design of an ultralight sailplane with a mean chord of only 0.5 meters prompted the need for a glider wing section with good performance characteristics at low Reynolds number. A 0.5 meter mean chord only represents about 25% decrease in Reynolds number compared to current competition sailplanes, but wing profile drag is sensitive to Reynolds number. A higher operating lift coefficient would allow the use of a higher wing loading that would partly compensate for

the smaller wing chord.

The design procedure could be described as computer aided design using computer codes developed at the University of Alberta (1), (2).

The bottom surface uses the flat bottom laminar-to-the-trailing-edge design that worked very well on the UA (2)-180 airfoil section (3). The top surface has a more conventional laminar roof top pressure distribution which maintains laminar flow to about 65% chord on the top surface, followed by a laminar separation bubble type transition and turbulent boundary layer pressure recovery. Transition will eventually move forward as the suction peak at the nose develops, and the resulting thick turbulent boundary layer results in a turbulent boundary layer separation starting at the trailing edge which moves forward only very slowly with increasing angle of attack. This provides very desirable gentle stall characteristics that will be important for flight safety. Computer modeling provides a facility for analysis of design changes and handling of data that allows the designer to tailor the airfoil characteristics, but wind tunnel tests are needed to confirm computer predictions and provide information on separated flow characteristics where the computer model results are not completely reliable.

This report gives wind tunnel results for a new glider wing section designated as UAG 88-143/20. This 14.3% thick section has a 20% chord camber changing flap. Tests were carried out in the University of Alberta low turbulence wind tunnel for Reynolds number 0.5×10^6, 1×10^6 and 2.1×10^6 with the camber flap at deflections of $\delta_f = +10$, 0 and -10. Some additional measurements were carried out with $\delta_f = -5$ at $Re = 1.0 \times 10^6$ and $\delta_f = -12.5$ at $Re = 2.1 \times 10^6$. These results were interpolated to provide profile drag as a function of lift coefficient at flight Reynolds numbers.

Tests with simulated insect roughness (bugs) were carried out to determine the sensitivity of the new wing section to roughness.

Equipment and procedures

Tests were carried out in the University of Alberta 1.22 x 2.44 meter wind tunnel. This is a closed-return wind tunnel with a low, free-stream turbulence level of less than 0.01 percent.

A one-meter chord model was mounted spanning the short dimension of the test section. The model was constructed with an 0.8 mm aluminum skin over a plywood framework with some styrofoam ribs to stabilize the metal skin. This technique produced a very accurate surface contour. The airfoil shape was within 1 mm of the correct shape (0.1% of chord), and there was no discernable waviness. The good contour accuracy of the model was confirmed by the lack of waviness in the measured pressure distributions. The model surface was painted black for flow visualization purposes. The surface was smoothed by wet sanding with 600 grit sandpaper. Flow visualization confirmed laminar flow back to the predicted location of laminar separation.

The model was equipped with a 20% chord plain flap with a blunt trailing edge. The trailing edge radius was approximately 0.4% of the wing chord.

The flap had a semi-circular nose and was fitted to the wing with gaps of about 3 mm to represent a practical construction. The gaps were sealed internally to prevent flow through the wing section at the flap. The shape of the UAG 88-143/20 wing section is shown in Figure 1.

Boundary layer control by suction through a distribution of holes in the mounting plates at the ends of the wing model was used to eliminate the formation of a wing tip vortex in the tunnel wall boundary layer and generally to ensure two-dimensional test conditions. Flow visualizations indicated that this was effective. Features such as laminar separation bubbles ran in straight lines across the entire span outside of the wall boundary layers.

Lift and moment coefficients were determined by integration of measured pressure distributions. Drag was determined from a pitot-static traverse through the wake at a location 1.5 chord lengths behind the model trailing edge. All measurements were made using a data acquisition system controlled by a small computer, which also carried out the data reduction converting measured voltages to pressure coefficients and performing the integrations needed to determine the aerodynamic coefficients. Standard wind tunnel corrections (4) were also calculated by the computer.

Insect roughness was simulated by attaching duct tape "bugs" in a pattern along the leading edge of the model. Each "bug" was approximately 4 mm square and 0.3 mm thick. They were spaced along the leading edge at intervals of 60 mm with additional rows on the top and bottom surfaces 20 mm back from the leading edge, with bugs spaced between the leading edge bugs.

UAG 88 - 143/20

Figure 1. Airfoil Shape

Flow visualization

Flow visualization was carried out using a mixture of kaolin and varsol, a variation of the oil film technique. The mixture dries quickly in areas of high shear, such as the turbulent boundary layer, and turns white to show up these areas. Laminar separations and reattachments are particularly well shown up by this method. The flow visualization material itself did not change the character of the boundary layer, as indicated by comparison with the pressure distributions, and theoretical predictions of the extent of laminar flow.

Results

Figure 2 shows lift coefficient C_L as a function of α. The very gentle stall characteristics due to the progressive trailing edge flow separation on the upper surface is evident from these figures.

Pitching moment about the quarter chord is shown in figure 3 for a range of angles of attack at $RE = 2.1 \times 10^6$ $C_{M1/4} \approx -14$ for zero flap, -0.24 for flap down 10°, and -0.03 for flap up 10^6, making $d C_{M1/4}/d\delta_f \approx -0.010$ for the flight regime where flow is attached. The relatively large value of $C_{M1/4}$ is

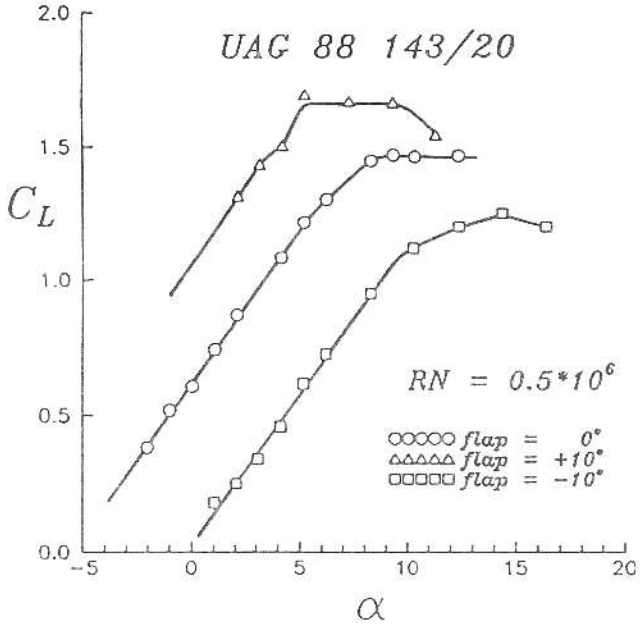

Figure 2. (a) Lift coefficient, RN = 0.5x10^6

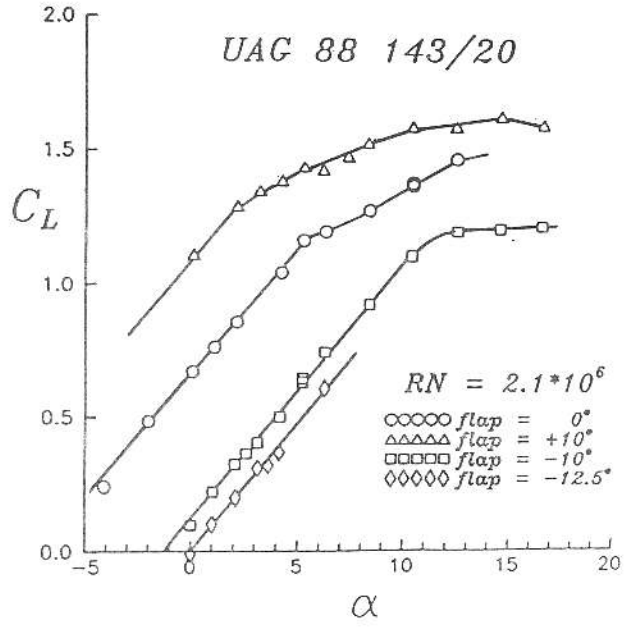

Figure 2. (c) Lift coefficient, RN = 2.1x10^6

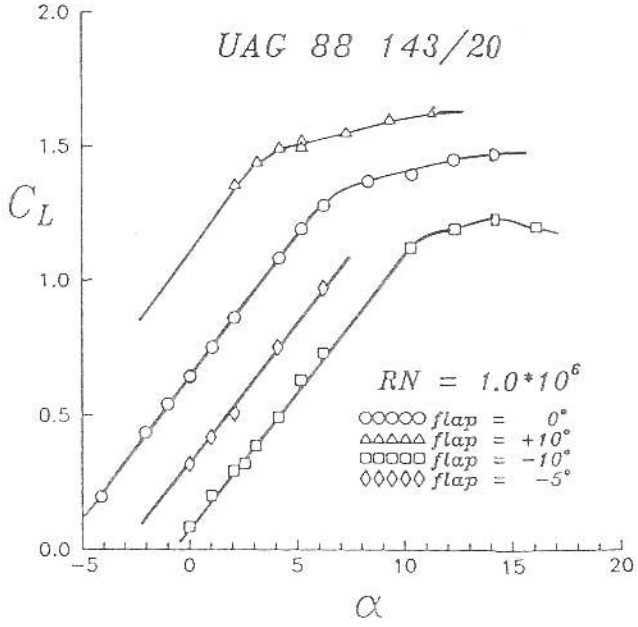

Figure 2. (b) Lift coefficient, RN = 1.0x10^6

associated with the large camber of this wing section.

Figure 4 shows C_L against C_D for the three test Reynolds numbers and various flap settings. The envelope of drag coefficient is nearly constant over a range of C_L from 0.3 to 1.5 for each Reynolds number. Intermediate flap settings would be needed for best results, as shown by the $\delta_f = -5°$ setting in figure 4(b). A flap setting more negative than $-10°$ would be appropriate for the highest flight speeds. The most negative flap setting tested was $\delta_f = -12.5°$, which would extend the low drag range down to $C_L = 0.25$ as indicated in figure 4(c). The pressure distribution shown in figure 5 indicates no flow separation on the flap lower surface with this negative setting.

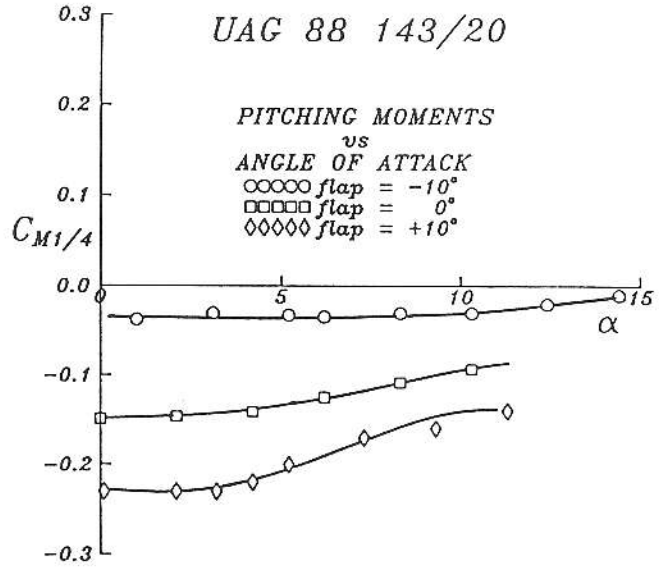

Figure 3. Moment Coefficient, RN = 2.1 X 10^6

Simulated insect roughness

At lower angles of attack, and especially at lower Reynolds number, the duct tape "bugs" have little effect on lift or drag. In particular, at Reynolds nmber 0.5 x 10^6 there was no change in lift or drag, virtually right up to maximum C_L. As Reynolds number and angle of attack increase, the laminar boundary layer near the leading edge becomes thinner, and the pressure gradient less favorable. Early transition due to roughness elements produces a thick turbulent boundary layer and separation near the trailing edge giving rise to sharply increased drag.

Flight Reynolds number

For any given aircraft the flight airspeed and hence Reynolds number, is inversely proportional to the square root of lift coefficient. This can be expressed as

$$R = \frac{R^*}{\sqrt{C_L}}$$

where $R^* = \frac{c}{\mu}\sqrt{2\rho W/S}$

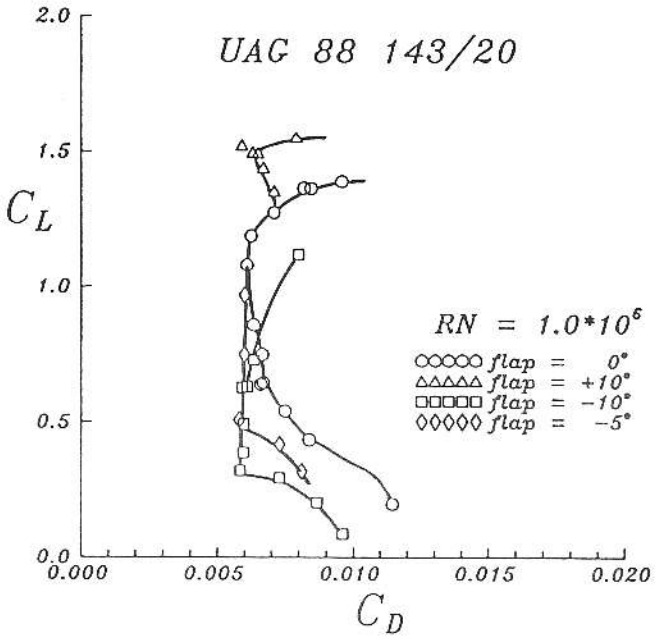

Figure 4. (b) C_L V_s C_D, RN = 1.0x10^6

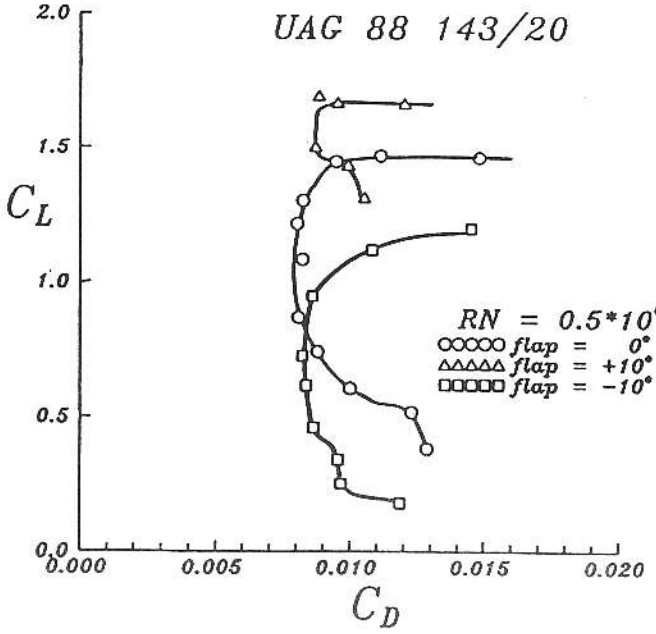

Figure 4. (a) C_L V_s C_D, RN = 0.5x10^6

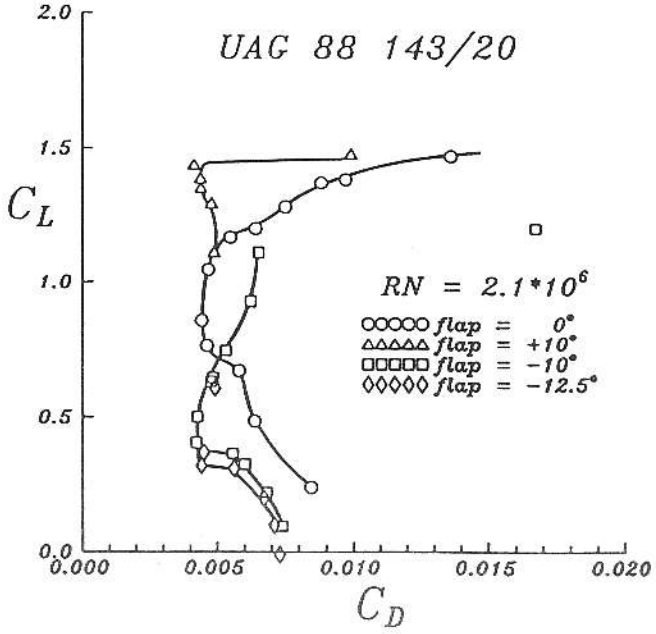

Figure 4. (c) C_L V_s C_D, RN = 2.1x10^6

c = wing chord
W = aircraft weight
S = wing area
ρ = air density
μ = viscosity of air

Airfoil characteristics are usually given for constant Reynolds number to be independent of particular aircraft characteristics. However, a brief survey of current racing sailplane types (Table 1) shows that they all have $R^* \approx 1.1 \times 10^6$ based on mean chord without water ballast and $R^* \approx 1.3 \times 10^6$ with water ballast to increase wing loading by 50%.

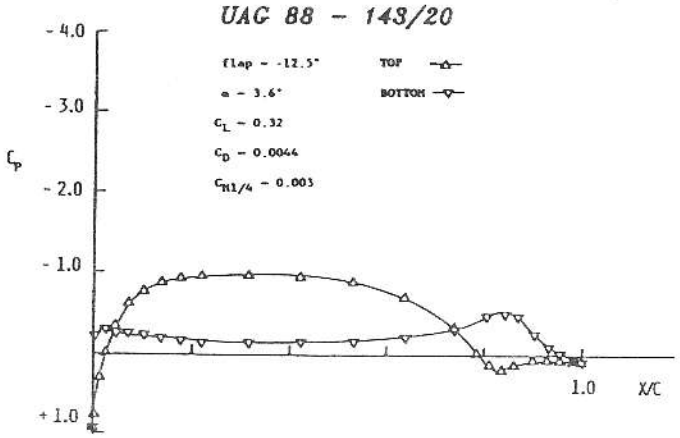

Figure 5. Measured Pressure Distribution with Flap Up 12.5°

Thus, it would be sensible to interpolate the constant Reynolds number data measured to provide wing section characteristics for constant values of R*, giving C_D as a function of C_L directly based on flight Reynolds number. While Reynolds number is only weakly dependent on wing loading within the range of variation of wing loading possible by the use of water ballast, there is typically a 2:1 variation in wing chord from root to tip which gives a much larger variation in R*. The data from Figs. 4(a), 4(b) and 4(c) have been interpolated to represent flight Reynolds numbers for three values of R*. $R^* = 1.7 \times 10^6$, corresponding to root chord with water ballast for a wing loading of 45 kg/m², $R^* = 0.7 \times 10^6$, representing tip chord without water ballast, W/S = 30kg/m², and $R^* = 1.1 \times 10^6$ representing mean chord at W/S = 30 kg/m².

Table 1
Values of R* based on mean chord

Sailplane	Mean Chord (m)	Approximate Wing Loading Range (kg/m²)	R*(Mean Chord)x10⁻⁶
Nimbus 3	0.68	28 - 45	0.99 - 1.25
ASW-20	0.70	32 - 45	1.09 - 1.29
Ventus	0.63	32 - 50	.98 - 1.23
Jantar Standard	0.72	32 - 45	1.12 - 1.33
DG-600	0.72	30 - 50	1.08 - 1.39
LS-3A	0.70	31 - 45	1.07 - 1.29
ASH-25	0.65	36 - 46	1.07 - 1.21
		Average	**1.06 - 1.27**

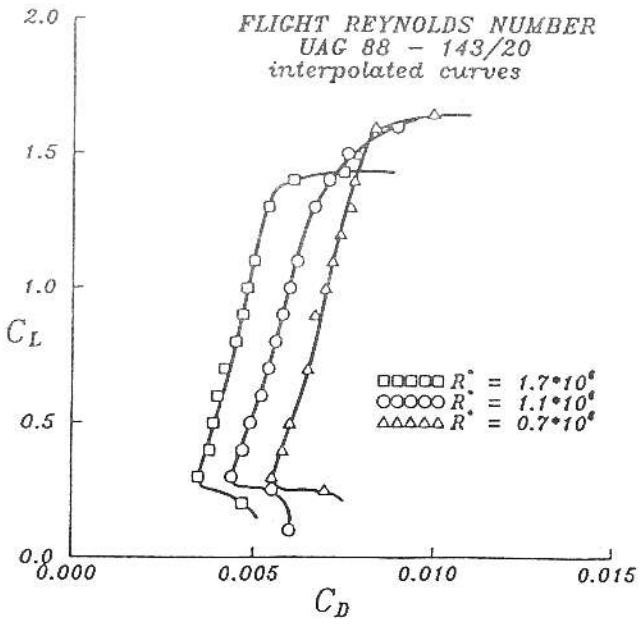

Figure 6. C_L Vs C_D with R* = constant

The result shown in Figure 6 is an interpolation of the measured results, each curve representing an envelope of results with adjustable camber flap from $\delta_f = +10°$ to $-10°$.

Figure 7 shows a similar interpolation of the results of the simulated insect roughness tests. Comparison with Figure 6 shows very little effect of rughness for the lowest value of R* representing tip chord at the lowest wing loading, but a very substantial increase in drag of the order of 75% for the highest value of R*. The middle value of R* representing mean chord without water ballast shows a 20% increase in drag at C_L = 0.5 dropping to zero at C_L = 1.0.

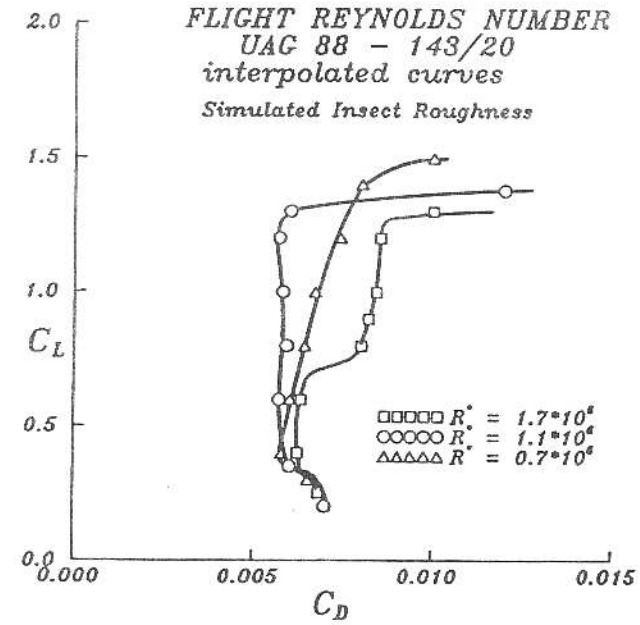

Figure 7. C_L Vs C_D with R* = constant and Simulated Insect Roughness

Comparison with other wing sections

There are not many published data on current sailplane wing sections available for comparison. Horstmann and Quast (5) give a flight Reynolds number drag polar curve for their HQ-17 wing section measured at Delft, together with data for the FX-62-K-131 and FX-67-K-150 wing sections. The value of R* for this figure appears to be approximately R* = 1.1 x 10^6. Figure 23 of Reference (5) is reproduced in Figure 8 with the addition of the data for US 88-143/20 at R* = 1.1 x 10^6.

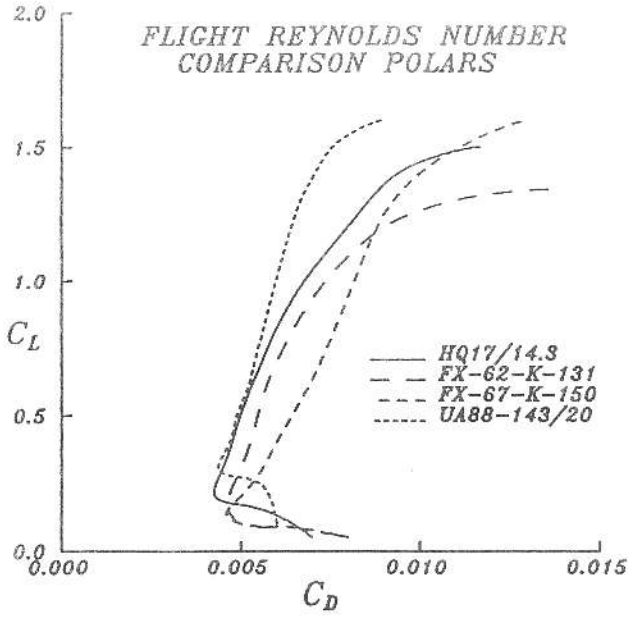

Figure 8. Comparison with other Sailplane Wing Sections.

Figure 9 shows a comparison of flight Reynolds number drag results for the UA 88-143/20 with the measured data for FX-67-K-150 (6) wing section. The FX-67-K-150 wing section was used on many sailplanes designed in the 1970's. It shows a strong dependence of drag on Reynolds number. The superior performance of the UAG 88-143/20 for low Reynolds number is very obvious and will be particularly important on wing tip sections where the chord is small.

Conclusion

A new sailplane wing section, UAG 88-143/20, was tested in the University of Alberta low speed wing tunnel. Results are shown in terms of flight Reynolds number which is inversely proportional to the square root of lift coefficient. A Reynolds number parameter $R^* = c/\mu \sqrt{2\rho W/S}$ was introduced to represent aircraft geometry and wing loading characteristics. R* is a constant equal to Reynolds number when $C_L = 1.0$. It was found that R* x 1.1 x 10^6 for all current generation racing sailplanes based on mean chord and no ballast. Taking into account wing taper and variation in wing loading from 30 kg/m^2 to 45 kg/m^2 values of R* could vary from 0.7 x 10^6 at the wing tip to 1.7 x 10^6 at the root with full ballast. Measured drag results

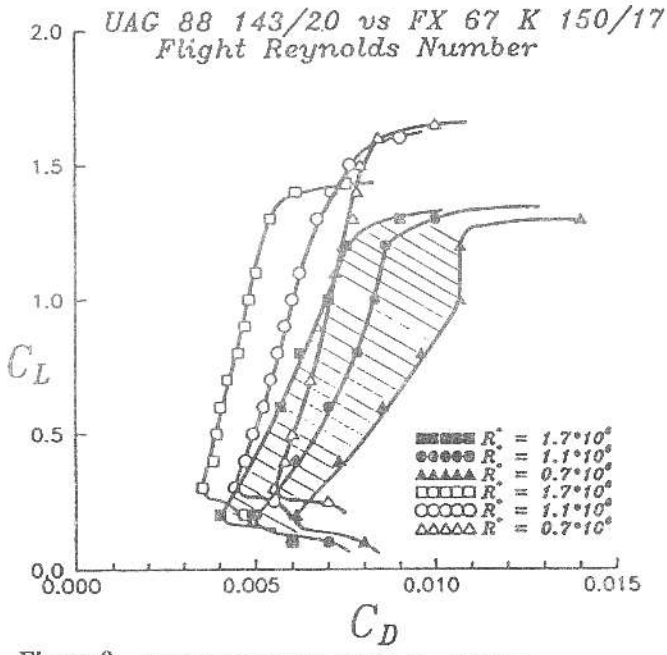

Figure 9. Comparison with FX 67-K - 150/17.

were interpolated to show flight Reynolds number polars over this range of values of R*.

Performance of this new wing section is compared with the HQ 17-143 and earlier FX airfoils for which more complete wind tunnel results have been published. The new airfoil appears to have better performance for C_L greater than 0.5 with particular advantage of higher C_L. The camber changing flap is needed to provide optimum performance over a wide speed range.

Some simulated insect roughness tests indicate a good tolerance to roughness, particularly at lower Reynolds number.

Other practical features of this new wing section include very gentle stall characteristics that will enhance flight safety, no under camber and a wedge shaped trailing edge to reduce control hinge moments, and no requirement for turbulators.

The UAG 88-143/20 wing section has excellent performance characteristics that would make it suitable for the proposed ultralight sailplane, or for use with any new sailplane.

References

1. Kennedy, J.L., "The Design and Analysis of Airfoil Section," Ph.D. Thesis University of Alberta, 1977.

2. Kennedy, J.L. and Marsden, D.J., "A Potential Flow Design Method for Multi-Component Airfoil Sections," Journal of Aircraft, Vol. 15, No. 1, 1978.

3. Marsden, D.J., "A High Lift Wing Section for Light Aircraft," Canadian Aeronautics and Space Journal Vol. 34 No. 1, March 1988.

4. Pope, Alan and Parker, John J. "Low Speed Wind Tunnel Testing," John Wiley & sons.

5. Horstmann, Karl-Heinz and Quast, Armin, "Drag Reduction by Means of Pneumatic Turbulators." European Space Agency Technical Translation ESA-TT-743 Sept. 1982.

6. Althaus, D. and Wortmann, F.X., "Stuttgarter Profilkatalog 1," 1972.